energy&fuels

Article

Cite This: Energy Fuels 2019, 33, 11454−11464

pubs.acs.org/EF

Highly Selective CO_2 Uptake in Novel Fishnet-like Polybenzoxazine-Based Porous Carbon

Lin Hong,[†] Shunlong Ju,[‡] Xiaoyun Liu,*[,†] Qixin Zhuang,[†] Guozhu Zhan,[§] and Xuebin Yu*[,‡]

[†]Key Laboratory of Specially Functional Polymeric Materials and Related Technology (ECUST), Ministry of Education, East China University of Science and Technology, Shanghai 200237, China

[‡]Department of Materials Science, Fudan University, Shanghai 200433, China

[§]The 806th Institute of the Eighth Academy of CASC, Huzhou 313000, China

Supporting Information

ABSTRACT: Porous activated carbons are considered to be promising CO_2 adsorbents due to their high specific surface area, high chemical stability, and tailorable surface properties. However, their low CO_2 capture capacity and inferior CO_2/N_2 selectivity have hindered their application. Here, we describe novel fishnet-like, polybenzoxazine-based porous carbons (PBZCs) prepared by a single-step monomer thermal curing, carbonization, and activation process. The PBZCs exhibit an ultrahigh CO_2 uptake capacity of 8.44 mmol g^{-1} and a superior CO_2/N_2 IAST selectivity of 56 (at 273 K, 1 bar). Such excellent CO_2 adsorption performance may to some extent be ascribed to a high specific surface area and a large ultramicropore volume. However, the results reveal that the CO_2 capture capacity is not solely associated with porosity. It may also be attributable to the abundant hydroxyl groups of the PBZCs, which may form hydrogen bonds with CO_2 molecules. The role of the oxygen functionalities of porous carbon for CO_2 capture was further demonstrated through theoretical calculation combined with experimental analysis. Hydrogen bonding lowers the binding energy between the carbon framework and CO_2 molecules, which greatly facilitates CO_2 adsorption. Furthermore, the novel fishnet-like structure can anchor CO_2 molecules effectively and selectively. These PBZC carbons are potentially promising CO_2 adsorbents.

1. INTRODUCTION

Fossil fuels are the primary energy source used in human technology, and their combustion produces CO_2 emissions. In recent decades, excessive CO_2 emissions have induced serious environmental problems such as global warming and ocean acidification.[1−7] Given the continuous global reliance on fossil fuels due to their low cost and accessibility, there is a pressing need to mitigate CO_2 emissions. To reduce the CO_2 level of the atmosphere, CO_2 capture and sequestration (CCS) techniques have attracted increasing attention.[8] Therefore, there are ongoing efforts to find materials that can effectively and selectively capture CO_2 from the atmosphere.

Currently, aqueous amine solutions are employed for the treatment of flue gases (mainly containing N_2 and CO_2). However, this conventional method has serious drawbacks such as toxicity, volatility, corrosion of the equipment, and energy-intensive regeneration.[9] To circumvent these issues, a number of porous CO_2 adsorbents, such as metal oxides,[10] zeolites,[11] metal−organic frameworks (MOFs),[12−14] covalent organic frameworks (COFs),[15] and porous carbons,[16−26] have been reported. Among these adsorbents, porous carbons are considered to be promising candidates for CO_2 capture because of their high surface area, tunable porosity, high stability, abundant resources, and tailorable surface properties.[27,28] The major drawbacks of commercial porous carbons are their moderate CO_2 capture capacity and low CO_2/N_2 selectivity, which have limited their practical application.

To deal with this problem, heteroatoms and functional groups can be incorporated into porous carbons to enhance CO_2 capture capacity and selectivity. N-doped porous carbons (NPCs) have been proven to have beneficial CO_2 capture properties and have been widely investigated for their application to CO_2 adsorption.[9,17,27,29−33] However, there have been differing accounts about the mechanism of the interaction between the CO_2 molecule and N-doped carbons. Wan et al. prepared a series of NPCs, which showed CO_2 uptakes of 4.02 and 6.35 mmol g^{-1} at 25 and 0 °C, respectively. They concluded that the incorporation of basic nitrogen functionalities into the network of porous carbons is beneficial for the uptake of acidic CO_2 gas.[29] Xing et al. synthesized N-enriched activated carbons derived from bean dreg.[34] The resulting sample showed a rather high CO_2 adsorption capacity of 4.24 mmol g^{-1} at 278 K and 1 bar. They utilized the hydrogen-bonding interaction between the hydrogen atoms (from CH and NH) and CO_2 molecules to explain the elevated CO_2 adsorption capacity.[34] In recent years, oxygen-containing porous carbons have attracted attention for CO_2 capture.[35−37] However, the impact of oxygen functionalities in CO_2 capture of porous carbon has been underestimated thus far. Oxygen-containing groups of porous organic polymers and MOFs have been proven to be favorable for CO_2 capture.[38−41] Knowledge of a detailed interaction mechanism of porous carbon oxygen functionality based on theoretical calculation and experimental analysis is lacking.

Received: August 7, 2019
Revised: October 3, 2019
Published: October 4, 2019

DOI: 10.1021/acs.energyfuels.9b02631
Energy Fuels 2019, 33, 11454−11464

A new class of high-performance thermosetting resins called polybenzoxazines (PBZs) is considered promising candidates for use with porous carbons. Compared to other precursors, polybenzoxazines show many advantageous properties, such as containing nitrogen and oxygen heteroatoms, excellent thermal stability, high char yield, and molecular design flexibility.[42−48] Polybenzoxazine molecules can be synthesized from inexpensive raw materials including primary amines, phenols, and formaldehyde. Therefore, the structure of the precursors can be easily modified by replacing various amines and phenols, which is desirable for adjusting the surface chemistry of porous carbons. More importantly, through the utilization of polybenzoxazine as the precursor of porous carbons, this technique can transform the poisonous formaldehyde into air purification products. Despite these advantages, the rational design of polybenzoxazine-based porous carbons for CO_2 capture has received little study.

In the present study, we report a new benzoxazine and find that its corresponding polybenzoxazine could be used to prepare novel fishnet-like polybenzoxazine-based porous carbons (PBZCs) by a simple and effective route. The rational design of the benzoxazine molecular structure can result in that each unit of corresponding polybenzoxazine contains three hydroxyl groups. Prepared PBZCs show an ultrahigh CO_2 uptake capacity of 8.44 mmol g^{-1} (273 K, 1 bar) and superior CO_2/N_2 selectivity of 56 (273 K, 1 bar). Notably, we found that CO_2 adsorption performance was not closely linked with the specific surface area and ultramicropore volume. To further reveal the relationship between CO_2 uptake properties and structures, quantum chemical calculations were carried out and it demonstrates that the hydrogen bonding interaction between porous carbon and CO_2 molecules provides strong CO_2 binding sites, which plays an important role in the enhancement of CO_2 adsorption capacity and CO_2/N_2 selectivity.

2. EXPERIMENTAL SECTION

2.1. Materials. 5-(4-Hydroxystyryl)benzene-1,3-diol (98%), aniline (AR grade), formaldehyde (37 wt % in water), ethanol (AR grade), potassium hydroxide (95%), hydrochloric acid (36−38 wt %), and sodium hydroxide (99%) were purchased from Sigma. All chemicals were used as received. All gases were purchased from Air Liquide (China) Holding Co., Ltd.

2.2. Preparation of Polybenzoxazine-Based Porous Carbons (PBZCs). A solution of 5-(4-hydroxystyryl)benzene-1,3-diol (2 g, 8.77 mmol), CH_2O (3.95 mL, 52.6 mmol), and aniline (2.40 mL, 26.3 mmol) in ethanol solution (100 mL) was stirred at room temperature for 12 h. After rotary evaporation, the ethanol was removed from the reaction mixture and then the product was washed with 100 mL of deionized water three times, followed by immersing in 1.0 M NaOH solution for 30 min to remove phenol residual. The yellow product was collected and dried under vacuum at 70 °C for 24 h to obtain the powder.

The prepared benzoxazine monomer was poured into ceramic models, and they were put into a tube furnace (OTF-1200X-S, Hefei Kejing Co., Ltd.). The monomer was cured by thermal treatment (5 °C/min), and the temperature programs were as follows: 120 °C (4 h), 140 °C (3 h), 180 °C (2 h), 200 °C (1 h), and 220 °C (1 h). After cooling to room temperature (5 °C/min), the cured polybenzoxazine was further carbonized in the same tubular furnace by heating at 500 °C for 1 h with a heating rate of 2 °C min^{-1}. The resulting carbonized material was denoted as PBZ-C.

Subsequently, the carbonized precursor mixed with KOH powder, and the mixtures were ground adequately for 30 min. By varying the activation conditions (activation agent mass ratio, time, and temperature), a series of porous carbon PBZCs were prepared. Among these PBZC-activated carbons, several samples own the optimal surface area, pore structure, and gas absorption property. The activation temperature was elevated at a ramp rate of 5 °C/min up to the setting temperature and held at this temperature for 1 h under Ar flow (100 mL/min). After cooling down to room temperature (5 °C/min), the products were poured into 1 M HCl solution and stirred for 30 min to remove KOH and inorganic salts. The samples were washed by HCl three times, followed by washing with plenty of deionized water until the PH value reached 7, and then immersed in absolute ethyl alcohol for 3 min and washed three times. The resulting polybenzoxazine (PBZ)-derived porous carbons were denoted as PBZC-3-T where the "3" represents the mass ratio of the KOH/carbonized precursor and "T" indicates the activation temperature.

2.3. Characterization. ^1H NMR spectra were recorded using an NMR spectrometer (Bruker, 400 MHz) with DMSO-d_6 as the solvent. FTIR spectra of the benzoxazine monomer and porous carbons were measured on a Bruker Tensor 27 FTIR spectrophotometer with a KBr wafer. X-ray diffraction (XRD) patterns were performed on a Bruker D8 Advance diffractometer with Cu Kα radiation (λ = 0.15406 nm). The surface topography of porous carbon was examined by scanning electron microscopy (SEM), which was recorded on a Hitachi S4800 microscope instrument operating at 5 kV. X-ray photoelectron spectroscopy (XPS) spectra were measured on an ESCALAB 250 spectrometer with an excitation source of Mg Kα (1486.6 eV). A Micromeritics ASAP 2020 analyzer was used to assess the pore structure and gas adsorption by measuring the isotherms for N_2 and CO_2 after degassing the porous carbons at 200 °C for 20 h. N_2 adsorption−desorption isotherms were carried out using high purity N_2 at 77 K. The specific surface area was calculated by the Brunauer−Emmett−Teller (BET) method, using the data from the N_2 adsorption isotherms. The pore size distribution (PSD) was obtained from the adsorption isotherms using the nonlocal density functional theory (NLDFT). The total pore volumes were derived from the adsorbed amount at a relative pressure of 0.99, and the micropore volume was estimated from the t-plot method. Gas adsorption experiments of CO_2 and N_2 were determined at 0 and 25 °C. Highly pure gases CO_2 and N_2 were employed for the measurements. To control the constant temperature precisely, the adsorption isotherms of CO_2 and N_2 at 273 K were measured in an ice−water bath and adsorption isotherms at 298 K were determined in a water bath. The dynamic breakthrough curves were recorded by a fixed-bed setup equipped with a gas chromatography (Shimadzu GC-2014) as a detector.

2.4. DFT Calculation. The calculations were performed in the framework of the density functional theory (DFT) using the projector-augmented wave (PAW) method as implemented in the Vienna ab initio simulation package (VASP).[49−51] The exchange and correlation energies were evaluated using the generalized gradient approximation (GGA) of the Perdew−Burke−Ernzerhof (PBE) functional,[52] and van der Waals (vdW) correction DFT-D2 proposed by Grimme was chosen to describe the long-range vdW interaction.[53] The energy cutoff was set to be 480 eV, and the 5 × 5 × 1 Monkhorst−Pack mesh for k points was employed for the Brillouin zone integration. The structures were relaxed using the conjugate gradient algorithm until the forces and total energy on all atoms were converged to less than 0.05 eV $Å^{-1}$ and 1 × 10^{-5} eV. The binding energy is used to evaluate the binding strength, which is defined as follows,

$$E_b = E_{substrate+CO_2} - E_{substrate} - E_{CO_2}$$

where $E_{substrate+CO_2}$, $E_{substrate}$, and E_{CO_2} represent the total energy of PBZCs, substrate, and CO_2 molecules, respectively.

3. RESULTS AND DISCUSSION

The precursor of the polybenzoxazine-based porous carbons was synthesized by the Mannich reaction and further thermal curing. Novel fishnet-like porous carbons were obtained after carbonization and activation (Figure 1). A Fourier transform infrared (FTIR) spectrum of the benzoxazine monomer was

DOI: 10.1021/acs.energyfuels.9b02631
Energy Fuels 2019, 33, 11454−11464

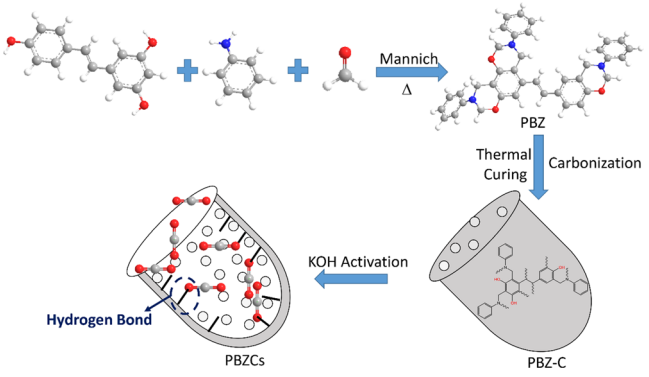

Figure 1. Schematic illustration of the fabrication of fishnet-like polybenzoxazine-based porous carbon.

recorded and is shown in Figure S1. The characteristic adsorption peaks of PBZ are located at 1234 cm^{-1} (symmetric stretching of C−O−C), 1071 cm^{-1} (asymmetric C−O−C stretching), 938 cm^{-1} (out-of-plane bending vibration of C−H), and 1600 cm^{-1} (stretching of C═C), which confirm the successful formation of benzoxazine rings.[29,43] The ^1H spectrum of the benzoxazine monomer is shown in Figure S2. In Figure S2, the benzoxazine monomer showed resonances at 4.6 ppm (O−CH_2−N) and 5.6 ppm (Ar−CH_2−N), which were consistent with the formation of the oxazine ring.

The pore morphology of the resulting PBZCs was characterized by scanning electron microscopy (SEM). As shown in Figure 2 and Figure S3a, the surface of PBZ-C is smooth without any wrinkles and pores when carbonized at 500 °C in the absence of KOH. For the sample PBZC-3-600, which was obtained in the presence of KOH, the surface has a low density of cavities that are several hundred nanometers in size (Figure 2a). A fishnet-like tube with plenty of pores on its wall can be observed for the sample PBZC-3-700, which can be attributed to the breakage of carbon−carbon single bonds in the polybenzoxazine-based precursor. As can be seen in the molecular structure of polybenzoxazine, the polymer exhibits plentiful carbon−carbon single bonds (Figure 1). Meanwhile, at higher temperatures, the surface deformation can be observed, producing a tunneling effect and forming the distinct fishnet-like structure. In addition, the unique fishnet-like architecture possibly relates to the choice of the polybenzoxazine monomer.

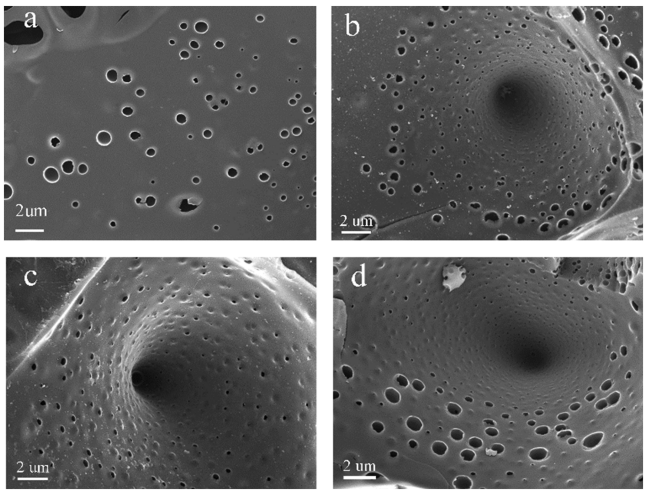

Figure 2. SEM images of samples: (a) PBZC-3-600, (b) PBZC-3-700, (c) PBZC-3-800, and (d) PBZC-3-900.

However, with an increased activation temperature in an alkali environment, more and more single bonds became extremely unstable, resulting in the formation of the pores on the wall of the fishnet-like structure. This may be explained by a higher KOH activation level occurring at elevated temperatures (Figure 2c). For the sample PBZC-3-900, we can observe that the macroporosity became more apparent compared with that of the other samples, which can be ascribed to the collapse of smaller pores at relatively high temperatures. Also, the corresponding optical photograph of the final PBZCs is shown in Figure S3.

The porous characteristics of the polybenzoxazine-based porous carbons were analyzed by nitrogen adsorption−desorption isotherms at 77 K, and the textural characteristics of the samples are listed in Table 1. All of the isotherms (Figure 3a) displayed a sharp increment in N_2 uptake at low pressures, followed by more even nitrogen adsorption in most of the pressure range, indicating that micropores were dominant in these porous carbons.[36] According to IUPAC classification, these isotherms of the PBZCs are characteristic of Type I. Notably, a slight hysteresis phenomenon can be observed in PBZC-3-600, indicating the existence of a small number of mesopores. However, as the temperature increases, the hysteresis phenomenon disappeared. The specific surface areas were calculated by the Brunauer−Emmett−Teller (BET) method and ranged from 816 to 2423 $m^2\ g^{-1}$. With increases in activation temperature from 600 to 900 °C, the BET surface areas increased rapidly. The sample PBZC-3-900 showed the highest surface area among all the PBZC samples, while samples PBZC-3-600, PBZC-3-700, and PBZC-3-800 had surface areas of 816, 1065, and 1414 $m^2\ g^{-1}$, respectively. A similar trend can be observed for the pore volume, which increases from 0.57 $cm^3\ g^{-1}$ (for PBZC-3-600) to 1.37 $cm^3\ g^{-1}$ (for PBZC-3-900). The pore size distributions of the PBZC samples are given in Figure 3b, calculated according to the nonlocal density functional theory (NLDFT). The micropore

Table 1. Textural Properties and Elemental Analysis of PBZCs

sample	S_{BET}[a] ($m^2\ g^{-1}$)	V_{TOT}[b] ($cm^3\ g^{-1}$)	V_{Mic}[c] ($cm^3\ g^{-1}$)	V_0[d] ($cm^3\ g^{-1}$)	C (wt %)	O (wt %)	N (wt %)
PBZC-3-600	816	0.53	0.51	0.47	76.20	18.74	2.03
PBZC-3-700	1065	0.65	0.64	0.58	80.40	14.5	1.92
PBZC-3-800	1414	0.86	0.78	0.63	83.21	12.92	0.82
PBZC-3-900	2423	1.47	1.36	1.15	89.15	8.46	0.17

[a]Brunauer−Emmett−Teller (BET) surface area. [b]Total pore volume at P/P_o = 0.95. [c]Calculated from the PSD and NLDFT models using the N_2 adsorption isotherm at 77 K. [d]Pore volume of ultramicropores (<0.7 nm) calculated from N_2 adsorption (273 K).

DOI: 10.1021/acs.energyfuels.9b02631
Energy Fuels 2019, 33, 11454−11464

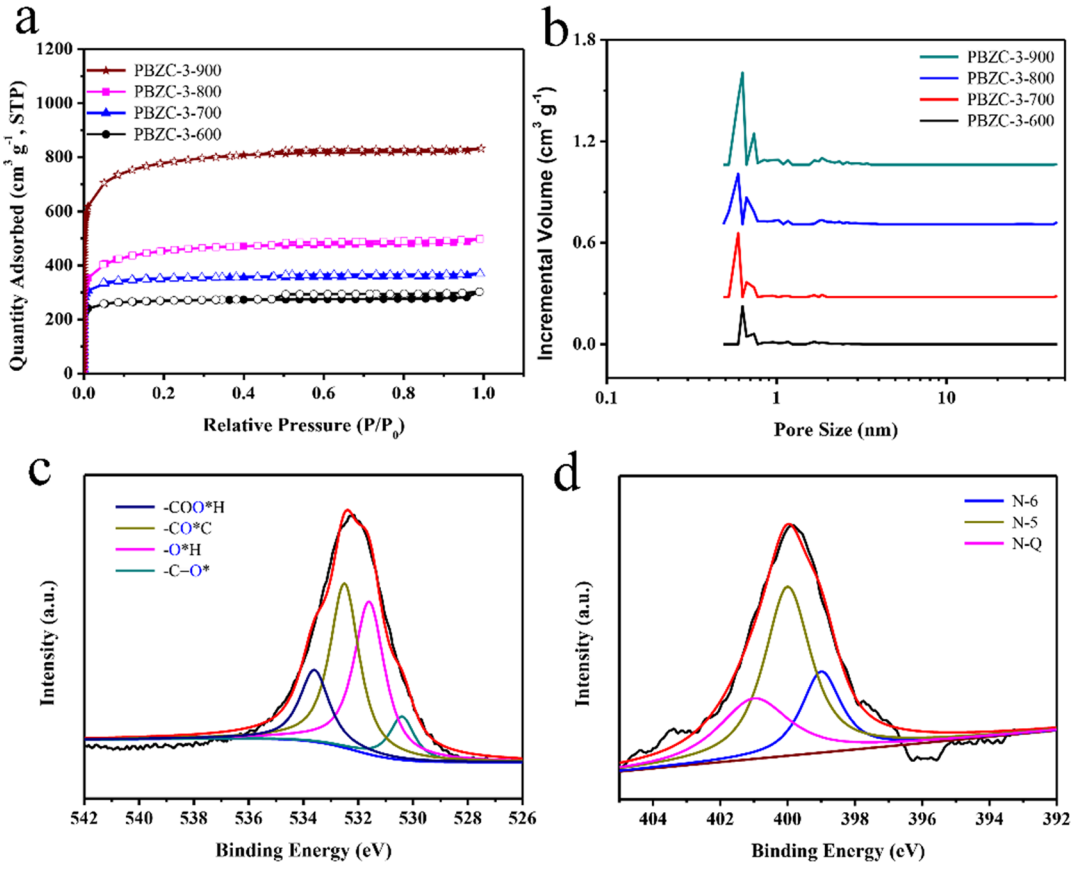

Figure 3. (a) N_2 adsorption isotherms and (b) pore size distribution. (c) O 1s and (d) N 1s X-ray photoelectron spectra of sample PBZC-3-800.

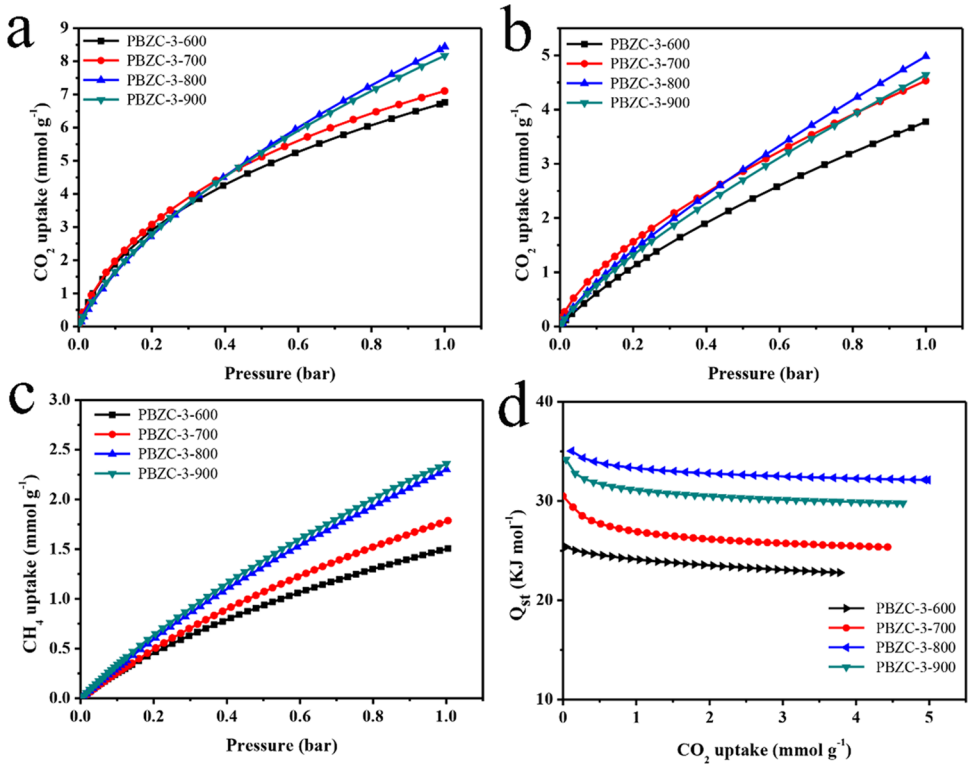

Figure 4. CO_2 adsorption isotherms at (a) 273 K and (b) 298 K for all samples. (c) CH_4 uptake isotherms at 273 K. (d) Isosteric heat of CO_2 adsorption for PBZCs.

DOI: 10.1021/acs.energyfuels.9b02631
Energy Fuels 2019, 33, 11454−11464

Table 2. Gas Uptakes (CO_2, CH_4, and N_2) at 1 bar and IAST Selectivity (CO_2/N_2 and CO_2/CH_4) for PBZCs

	CO_2 uptake (mmol g^{-1})		CH_4 uptake (mmol g^{-1})	N_2 uptake (mmol g^{-1})		IAST selectivity[a] CO_2/N_2 (10:90)		IAST selectivity[b] CO_2/CH_4 (50:50)
sample	273 K	298 K	273 K	273 K	298 K	273 K	298 K	273 K
PBZC-3-600	6.67	3.78	1.42	0.43	0.18	35	20	7.9
PBZC-3-700	7.10	4.43	2.11	0.53	0.27	56	59	7.2
PBZC-3-800	8.44	4.98	2.18	0.58	0.38	34	25	7.4
PBZC-3-900	8.17	4.64	2.60	0.67	0.35	37	31	6.2

[a]Calculated by IAST (273 and 298 K) for the gas mixture of 0.1:0.9 CO_2/N_2 at 1 bar. [b]Calculated from IAST (273 K) for the gas mixture of 0.5:0.5 CO_2/CH_4 at 1 bar.

Table 3. Comparison of the Performance of Various Adsorbents

sample	type of samples[a]	BET (m^2 g^{-1})	V_{micro} (cm^3 g^{-1})	$V_{ultramicro}$ < 0.7 nm (cm^3 g^{-1})	N (wt %)	CO_2 uptake at 1 bar (mmol g^{-1}) 273 K	298 K	IAST[b] CO_2/N_2	reference
PBZC-3-700	PCs	1065	0.64	0.58	1.92	7.10	4.43	59:1	this work
PBZC-3-800	PCs	1414	0.78	0.63	0.82	8.44	4.98	25:1	this work
SU-MAC-600	NPCs	1500	0.50	0.27	4.0	6.49	4.50	22:1	52
UC-650-2	NPCs	1394	0.52	0.65 (<1 nm)	1.64	6.67	4.4	12:1	63
NPC-2	NPCs	1255.9	0.52		5.21	6.35	4.02	32:1	29
sOMC	MCs	2255					2.0	10:1	64
A-NMC	NMCs	1417	0.40		6.7		3.2		65
CN-950	NPCs	1979			4.32		4.3	12:1	66
CP-2-600	PCs	1700	0.74	0.21	10.14	6.2	3.9	9:1	57
AS-2-600	PCs	1260	0.55	0.52		6.1	4.8	9:1	67
VR-93-M	PCs	2895	1.28	0.8		5.5	4.59	7:1	68
NG7	NPCs	979.6	0.412		4.19		2.7	18:1	69
CPC-550	NPCs	1630	0.59	0.35	7.88	8.3	5.8	21:1	55

[a]PCs represent porous carbons; NPCs represent N-doped porous carbons; MCs represent mesoporous carbons; and NMCs represent N-doped mesoporous carbons. [b]Calculated by IAST (298 K) for a gas mixture of 0.1:0.9 CO_2/N_2 at 1 bar.

sizes in all samples were similar, in the range 0.5−0.7 nm, which has been proven to be greatly beneficial for CO_2 capture.[37] As the activation temperature increases, the density of ultramicropores (d < 0.7 nm) increases. At a higher temperature, the chemical activation became more drastic, generating more ultramicropores in the porous carbons. A certain number of larger pores (maximum = 2 nm) were detected, resulting from the collapse of the porous carbon framework at higher temperatures. The sample PBZC-3-900 showed more ultramicropores than other samples. It had an ultramicropore volume of 1.12 cm^3 g^{-1} and the highest BET surface area.

According to previous reports,[54,55] the capacity of CO_2 uptake is related to the surface chemical composition of activated carbon. To reveal the nature of nitrogen and oxygen on the surface of activated carbon, X-ray photoelectron spectroscopy (XPS) was applied, as presented in Figure S4 and Table S1. The samples consisted of C, N, and O, which were detected by analyzing their 1s spectra. The oxygen contents of the different samples ranged from 8.46 to 18.74 wt %. The O 1s spectra included four peaks that were attributed to (O-I) carboxylic C═O, (O-II) hydroxyl OH, (O-III) phenol type C═OH/C−O−C, and (O-IV) carboxylic C═O—O*H, with binding energies of 530.4, 531.6, 532.5, and 533.6 eV, respectively.[37] The N 1s spectra of all samples showed three peaks at 399, 400, and 401 eV, which correspond to pyridinic N (N-6), pyrrolic N or pyridonic N (N-5), and quaternary N (N-Q), respectively.[34,56] The nitrogen and oxygen contents are closely linked to the activation temperature, indicating that the contents of N and O decrease dramatically at high temperatures, which is in accordance with previous literature.[34,56] The contents of O-containing and N-containing functionalities of all the samples were calculated (Table S1), and they indicate that hydroxyl and phenol were the abundant O-containing groups in these samples. As for N-containing groups, pyridinic N was the richest among most samples, whereas PBZC-3-800 possessed the most abundant pyrrolic/pyridonic N (N-5). According to previous literature, pyrrolic and pyridonic nitrogens (N-5) are considered to have stronger interactions with CO_2 molecules.[56,57] However, the sample PBZ-3-800 only contained 0.41 wt % pyrrolic/pyridonic nitrogen, which may have a slight influence on CO_2 uptake. Notably, the contents of hydroxyl and phenol reached 9.68 wt %.

The CO_2 capture performance of the PBZCs was investigated at 273 and 298 K at 1 bar. The CO_2 adsorption isotherms at 273 and 298 K are shown in Figure 4a,b, and the corresponding uptake values at 1 bar are presented in Table 2. It can be observed that the CO_2 uptake capacity of the PBZC-3-T samples first increased and then decreased as the activation temperature increased from 600 to 900 °C. Among these samples, at 1 bar, the sample PBZC-3-800 exhibited the highest CO_2 uptake capacities of 8.44 and 4.98 mmol g^{-1} at 273 and 298 K, respectively. Notably, PBZC-3-900 possessed the highest specific surface area and largest ultramicropore volume but exhibited a lower CO_2 capacity (8.17 mmol g^{-1})

DOI: 10.1021/acs.energyfuels.9b02631
Energy Fuels 2019, 33, 11454−11464

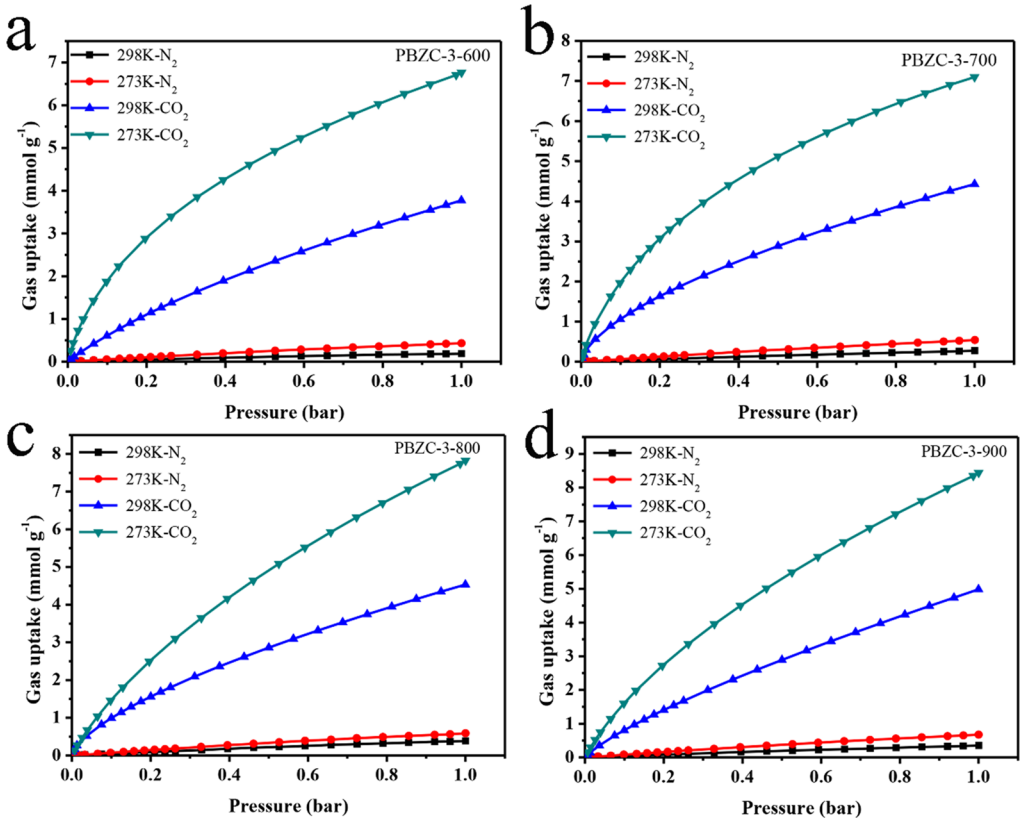

Figure 5. CO_2 and N_2 adsorption isotherms of PBZCs at 273 and 298 K.

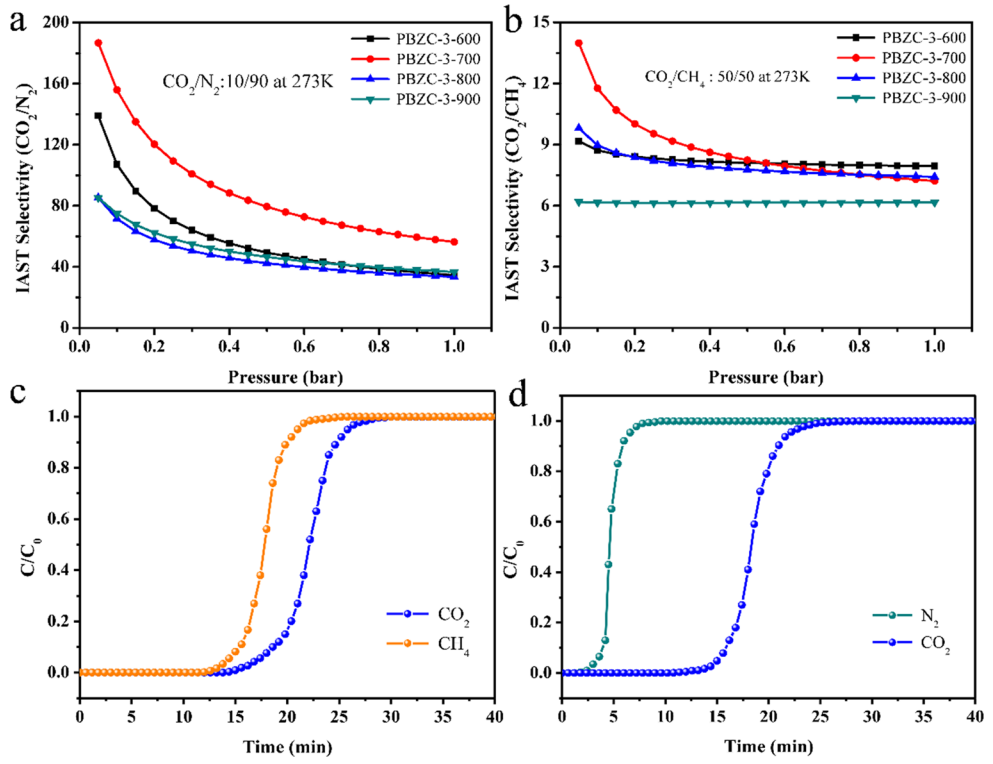

Figure 6. IAST selectivity analyses for (a) CO_2/N_2 and (b) CO_2/CH_4 at 273 K. Breakthrough curves for PBZC-3-700 at 298 K for different binary mixed gas: (c) CO_2/CH_4 (50:50) and (d) CO_2/N_2(10:90).

than that of PBZC-3-800 (8.44 mmol g^{-1}), indicating that the CO_2 capture capacity is not completely dependent on the porosity of the adsorbent. The surface chemistry may play an important role in the CO_2 adsorption performance. The adsorption capacity of the sample PBZC-3-800 is one of the highest yet reported among the polybenzoxazine-based nitro-

DOI: 10.1021/acs.energyfuels.9b02631
Energy Fuels 2019, 33, 11454−11464

gen-doped porous carbons, such as NPC-1 (6.20 mmol g^{-1} at 273 K),[58] NPC-2 (6.35 mmol g^{-1} at 273 K),[29] BZCN-A (2.82 mmol g^{-1} at 298 K),[59] and CBD-900 (5.16 mmol g^{-1} at 273 K).[60] The sample PBZC-3-600 showed the lowest CO_2 adsorption capacity of 6.76 mmol g^{-1} at 1 bar/273 K, which is still much higher than that of NPC-2. This indicates that the CO_2 capture performance of PBZCs is apparently superior to that reported for polybenzoxazine-based carbons. The high CO_2 uptake capacity of 8.44 mmol $g^{-1}$is also superior to that reported for different types of porous carbons under identical measurement conditions (Table 3). Compared to other types of porous carbons, the CO_2 uptake capacity of PBZCs, especially at 273 K, is among the highest reported under identical measurement conditions, although it is still lower than that of physically activated polyacrylonitrile (11.5 mmol g^{-1}).[61]

To explore CO_2/N_2 selectivity performance, N_2 uptake isotherms were collected at 273 and 298 K at 1 bar. As shown in Figure 5a and Table 2, the N_2 adsorption capacities of PBZC-3-600 are 0.43 and 0.18 mmol g^{-1} at 273 and 298 K, respectively, which are apparently lower than that for CO_2, indicating remarkable selectivity performance for CO_2 uptake against N_2.

Methane is generally utilized as a fuel and usually contains some acid gas CO_2, which can corrode equipment and compromise its heat value during the combustion process. Therefore, the capture of CO_2 from CH_4 has drawn much attention. The CH_4 isotherms were measured for all PBZC samples at 273 K up to 1.0 bar and are presented in Figure 4c. The values obtained from these samples all reveal excellent selective adsorption results of CO_2 from CH_4, ranging from 1.42 to 2.60 mmol g^{-1}. In the case of PBZC-3-800, its CO_2 capture capacity can reach 8.44 mmol g^{-1} at 273 K (1.0 bar); however, the uptake of CH_4 is only 2.18 mmol g^{-1}, which is much lower than that of CO_2. These results demonstrate that PBZCs can effectively separate CO_2 from methane-containing gas mixtures.

Based on the above results, the performance of PBZCs is considered ideal for the selective uptake of CO_2 from N_2 and CH_4 and may have the potential for application to gas separation. Landfill gas and flue gas are typically mixtures of CO_2/CH_4 and CO_2/N_2, respectively. Methods of removing CO_2 from N_2 and CH_4 are of great practical significance. We used the ideal adsorbed solution theory (IAST) to estimate the selectivity performance of CO_2/N_2 and CO_2/CH_4. Accordingly, a 10:90 mixture of CO_2/N_2 was calculated, and the selectivity results are displayed in Figure 6a. The IAST selectivity results for a 15:85 mixture of CO_2/N_2 are presented in Figure S4 and Table S2.

Specifically, the PBZC-3-T (T = 600, 700, 800, and 900) series showed IAST selectivity factors of 35, 56, 34, and 37 at 273 K (1.0 bar), respectively. Notably, at 273 K and 1.0 bar, the IAST selectivity remains high, ranging from 20 to 59, indicating that PBZC-3-T could effectively separate CO_2 from flue gas at room temperature. The IAST selectivity factor of 59 is comparable to the highest reported for porous carbon, as presented in Table 3. The values of CO_2/CH_4 IAST selectivity at 273 K (1 bar) ranged from 6.2 to 7.9, assuming a 50:50 mixture of CO_2/CH_4 (Figure 6b), which are close to those of PYDCs[8] and Zeolite-13X.[62] It is noteworthy that the IAST selectivity of CO_2/CH_4 is much lower than that of CO_2/N_2 selectivity, corresponding to a higher uptake capacity and the polarity of its methane molecules.

Based on the IAST selectivity, PBZC-3-700 shows higher selectivity toward binary mixed gases. To estimate the properties of PBZC-3-700 in the practical separation process, we carried out dynamic breakthrough experiments under kinetic flow conditions with a gas flow rate of 2 mL min^{-1} at 298 K. A gas chromatography was employed to detect the concentration of gas mixtures. As shown in Figure 6d, N_2 first eluted through the packed column due to its lower capacity and the CO_2 breakthrough occurs at about 14.4 min for CO_2/N_2 (10:90); thus, a clean separation of the gas mixture could be achieved. For CO_2/CH_4 (50:50) mixtures (Figure 6c), the breakthrough time for CH_4 was shorter compared to that of CO_2, indicating a high selectivity for landfill gas in a practical setting. Correspondingly, the gas mixture breakthrough selectivities of PBZC-3-700 were calculated to be 46 and 6.8 for flue gas (10:90) and landfill gas (50:50), respectively. These excellent results strongly demonstrated that the PBZC-3-700 is a promising CO_2 capture candidate for efficiently selective separation binary gas mixtures.

To further evaluate the interaction strength between CO_2 and the PBZC samples, isosteric heats of adsorption (Q_{st}) were calculated by Clausius−Clapeyron equations using CO_2 adsorption values measured at 273 and 298 K (Figure 4d). The values of Q_{st} reflect the binding affinity between CO_2 molecules and carbon, with higher values representing stronger interaction. PBZC-3-800 showed a high Q_{st} value, ranging from 32 to 35 kJ mol^{-1}, which apparently drops with the increases in loading. Similar downward trends in Q_{st} were observed for all samples, which could result from the changes in the interaction between CO_2 and the porous carbon surface binding sites. At low pressures, CO_2 molecules adequately interact with the heteroatoms of the carbon surface through hydrogen bonding and CO_2 molecules can be readily confined in the ultrafine pores, whereas the interaction strength decreases significantly as the binding sites become fewer and more saturated, which leads to downtrends in Q_{st} at higher CO_2 loadings. Furthermore, the moderate Q_{st} values of PBZCs not only provide a favorable binding affinity for CO_2 uptake but also a simple adsorbent regeneration method without high temperature, which could save regeneration costs for large-scale CCS processes.

Their ultrahigh CO_2 adsorption capacity makes PBZCs among the most promising candidates for use as CO_2 adsorbents. According to previous reports, gas uptake capacity generally depends on the specific surface area and microporosity of porous carbons. However, while PBZC-3-900 possessed the highest specific surface area (2423 m^2/g) and ultramicropore volume (1.12 cm^3 g^{-1}), it had a CO_2 adsorption capacity of 8.17 mmol g^{-1} (at 273 K and 1 bar), which is much lower than that of PBZC-3-800 (8.44 mmol g^{-1}) under identical conditions.

These results indicate that CO_2 capture capacity is not completely dependent on the specific surface area and ultramicropore volume of the adsorbent. Although a high specific surface area and large ultramicropore volume may affect the adsorption capacity to some extent, the ultrahigh CO_2 capacity of PBZCs cannot be solely explained by porosity. In this case, the major influence on ultrahigh capacity could be heteroatom doping. The effect of nitrogen functionalities on the enhancement of CO_2 adsorption capacity in porous carbons has been adequately documented.[32,33] Many authors have explained that heteroatoms can cause CO_2 molecule interactions with nitrogen functionalities through Lewis acid−

DOI: 10.1021/acs.energyfuels.9b02631
Energy Fuels 2019, 33, 11454−11464

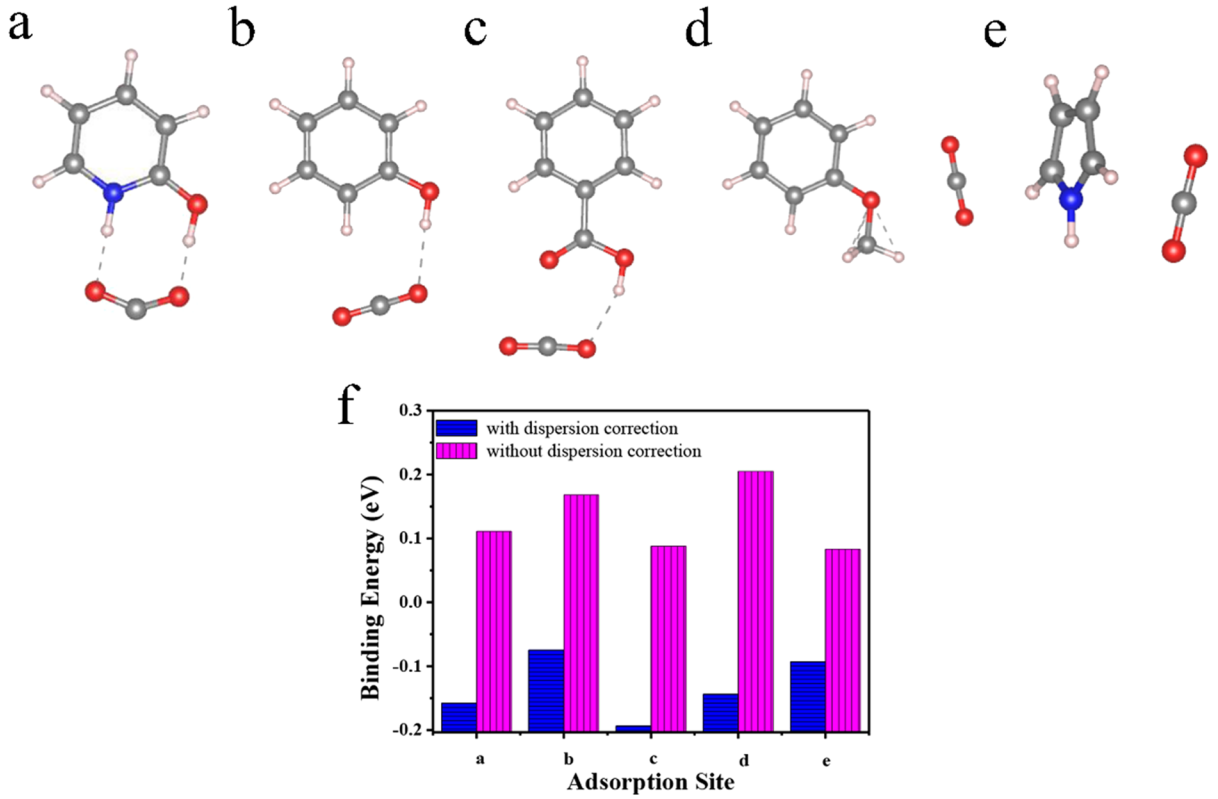

Figure 7. Adsorption structure between CO_2 and substrate with (a) pyridonic, (b) hydroxyl OH, (c) carboxylic, (d) methoxyl, and (e) pyrrolic N (gray, blue, red, and white balls represent C, N, O, and H atoms, respectively). (f) Binding energy with and without dispersion corrections.

base and dipole−quadrupole interactions. It is worth noting that PBZC-3-T possesses a trace nitrogen content that can be ignored, as it would hardly contribute to CO_2 uptake. In contrast, the oxygen content of PBZCs is much higher than that of nitrogen. The impact of oxygen-containing groups on the CO_2 uptake of carbons has been underestimated thus far. Notably, the precursor of PBZCs is derived from polybenzoxazine, which contains three hydroxyl groups. According to XPS analysis, abundant hydroxyl groups remained in the PBZC samples after high-temperature processing (Figure S5).

The introduction of electron-rich oxygen functionalities (especially hydroxyl groups) could obviously change the electron distribution of porous carbon, inducing polarity into the carbon framework. The oxygen-containing groups, as electronegative species, could anchor CO_2 molecules through hydrogen bonding interactions between the hydrogen atoms on the surface of the carbon (in OH and COOH) and the oxygen atoms of CO_2 molecules. The existence of hydrogen bonding greatly facilitates CO_2 adsorption capacity, which can explain the ultrahigh CO_2 capture capacity of PBZC-3-800. Furthermore, the presence of hydrogen bonding has a positive impact on CO_2/N_2 selectivity. Due to the difference between N_2 and CO_2, CO_2 molecules can form hydrogen bonds with PBZC porous carbons but there are no strong interactions between N_2 and carbons. This leads to an ultrahigh CO_2 capture capacity with a low N_2 capture capacity. Such huge adsorption variations contribute to high CO_2/N_2 selectivity performance. Both high CO_2 capture capacity and good CO_2/N_2 selectivity are deeply influenced by hydrogen bonding interactions, which make our materials highly promising for selective CO_2 capture from gas mixtures.

To further reveal the detailed interaction mechanism of the oxygen functionalities of porous carbon for CO_2 capture, DFT calculation was conducted to characterize the hydrogen bonding interactions between PBZCs and CO_2 molecules. Classic DFT calculation only takes strong interactions into account, that is, covalent and ionic bonds. However, dispersion interactions are totally neglected, such as hydrogen bonds and van der Waals forces. Therefore, DFT-D2 proposed by Grimme in which dispersion interactions such as hydrogen bonding and van der Waals forces are considered was employed to evaluate the hydrogen bond interactions between porous carbon and CO_2. We calculated the binding energy with and without dispersion corrections. The effect of hydrogen bonding can be reflected by the difference in the binding energies. As hydrogen bonds originate from the functional groups instead of the carbon framework, the carbon framework can be substituted by a benzene ring in the simulation.[37] The adsorption structures derived from the DFT calculations are presented in Figure 7, and the corresponding binding energies are listed in Table S3. The calculated binding energies with dispersion correction are all negative, while those without dispersion correction are all positive. According to the definition of binding energy, a negative binding energy suggests a stable adsorption structure, while a positive one indicates that CO_2 molecules cannot be adsorbed by the substrate. Although a simplified model was used, which cannot fully explain the adsorption of CO_2 molecules, the trend in the calculated binding energy shows that long-range hydrogen bonding is favorable to CO_2 uptake.

Based on the above DFT calculations, we demonstrate that the existence of hydrogen bonding reduces the binding energy between PBZCs and CO_2 molecules, which greatly enhances

DOI: 10.1021/acs.energyfuels.9b02631
Energy Fuels 2019, 33, 11454−11464

CO_2 adsorption. These results can explain the phenomenon whereby CO_2 uptake capacity is not closely linked with porosity. Similarly, the CO_2 adsorption performance of oxygen-doped porous carbon cannot be solely measured in terms of porosity, but should also take hydrogen bonding into account. Due to their high porosity, fishnet-like structure, and hydrogen bonding, PBZCs have an ultrahigh CO_2 capacity of 8.44 mmol g^{-1} and a superior CO_2/N_2 IAST selectivity of 56 at 273 K and 1 bar.

4. CONCLUSIONS

In conclusion, novel, fishnet-like PBZCs were prepared by the rational design of a modified polybenzoxazine precursor containing three hydroxyl groups. Specifically, the PBZCs were obtained by one-step monomer thermal curing, carbonization, and activation of a PBZ-KOH powdery mixture. The resulting porous carbons exhibit ultrahigh CO_2 uptakes of up to 8.44 mmol g^{-1} at 273 K and 1 bar. As the activation temperature increases, the porosity of the PBZCs increases significantly, which increases the N_2 and CH_4 adsorption capacities. However, CO_2 uptake was not completely positively correlated with porosity. Through theoretical calculation and experimental analysis, we have demonstrated the impact of the oxygen functionalities of PBZCs on CO_2 capture; these functionalities form hydrogen bonds with CO_2 molecules. The binding energies between porous carbons and CO_2 molecules are much lower with dispersion correction than without it. This indicates that the hydrogen bonding greatly facilitates CO_2 adsorption, enhancing both CO_2 uptake capacity and adsorption selectivity. Hence, the superior CO_2 adsorption performance is greatly influenced by hydrogen bonding, rather than being solely dependent on porosity. Furthermore, the fishnet-like framework of PBZCs effectively boosts the process of CO_2 capture. Such porous carbon PBZCs are promising CO_2 adsorbents, and our work provides a guidance for the design of new high-performance CO_2 adsorbents.

■ ASSOCIATED CONTENT

Supporting Information

The Supporting Information is available free of charge on the ACS Publications website at DOI: 10.1021/acs.energyfuels.9b02631.

FTIR and ^{1}H NMR spectra, SEM and optical images, 1s XPS spectrum, element contents of PBZCs, IAST selectivity studies, and comparison of calculated binding energy with and without dispersion corrections (PDF)

■ AUTHOR INFORMATION

Corresponding Authors

*E-mail: liuxiaoyun@ecust.edu.cn. Phone: 086-2164252464 (X.L.).

*E-mail: yuxuebin@fudan.edu.cn. Phone: 086-2155664581 (X.Y.).

ORCID

Xiaoyun Liu: 0000-0002-9838-1109

Xuebin Yu: 0000-0002-4035-0991

Notes

The authors declare no competing financial interest.

■ ACKNOWLEDGMENTS

This work was financially supported by the National Natural Science Foundation of China (51573045, 51625102, and 51773060), Shanghai Natural Science Foundation (16ZR1407700), Shanghai Rising-Star Program (17QB1401200), and the Fundamental Research Funds for the Central Universities (50321041917001).

■ REFERENCES

(1) Davis, S. J.; Caldeira, K.; Matthews, H. D. Future CO_2 Emissions and Climate Change from Existing Energy Infrastructure. *Science* **2010**, *329*, 1330−1333.

(2) Gadipelli, S.; Patel, H. A.; Guo, Z. An Ultrahigh Pore Volume Drives Up the Amine Stability and Cyclic CO_2 Capacity of a Solid-Amine@Carbon Sorbent. *Adv. Mater.* **2015**, *27*, 4903−4909.

(3) Alahmed, A. H.; Briggs, M. E.; Cooper, A. I.; Adams, D. J. Post-synthetic fluorination of Scholl-coupled microporous polymers for increased CO_2 uptake and selectivity. *J. Mater. Chem. A* **2019**, *7*, 549−557.

(4) Oschatz, M.; Antonietti, M. A search for selectivity to enable CO_2 capture with porous adsorbents. *Energy Environ. Sci.* **2018**, *11*, 57−70.

(5) Gadipelli, S.; Lu, Y.; Skipper, N. T.; Yildirim, T.; Guo, Z. Design of hyperporous graphene networks and their application in solid-amine based carbon capture systems. *J. Mater. Chem. A* **2017**, *5*, 17833−17840.

(6) Natarajan, S.; Bajaj, H. C.; Aravindan, V. Template-free synthesis of carbon hollow spheres and reduced graphene oxide from spent lithium-ion batteries towards efficient gas storage. *J. Mater. Chem. A* **2019**, *7*, 3244−3252.

(7) Pu, K.; Yang, Y.; Qu, X.; Gao, M.; Liu, Y.; Pan, H. Room Temperature Conversion of Carbon Dioxide into Fuel Gases by Mechanochemically Reacting with Metal Hydrides. *ChemistrySelect* **2017**, *2*, 5244−5247.

(8) Abdelmoaty, Y. H.; Tessema, T.-D.; Norouzi, N.; El-Kadri, O. M.; Turner, J. B. M.; El-Kaderi, H. M. Effective Approach for Increasing the Heteroatom Doping Levels of Porous Carbons for Superior CO_2 Capture and Separation Performance. *ACS Appl. Mater. Interfaces* **2017**, *9*, 35802−35810.

(9) Wang, L.; Rao, L.; Xia, B.; Wang, L.; Yue, L.; Liang, Y.; DaCosta, H.; Hu, X. Highly efficient CO_2 adsorption by nitrogen-doped porous carbons synthesized with low-temperature sodium amide activation. *Carbon* **2018**, *130*, 31−40.

(10) Sun, J.; Liang, C.; Tong, X.; Guo, Y.; Li, W.; Zhao, C.; Zhang, J.; Lu, P. Evaluation of high-temperature CO_2 capture performance of cellulose-templated CaO-based pellets. *Fuel* **2019**, *239*, 1046−1054.

(11) Bae, T. H.; Hudson, M. R.; Mason, J. A.; Queen, W. L.; Dutton, J. J.; Sumida, K.; Micklash, K. J.; Kaye, S. S.; Brown, C. M.; Long, J. R. Evaluation of cation-exchanged zeolite adsorbents for post-combustion carbon dioxide capture. *Energy Environ. Sci.* **2013**, *6*, 128−138.

(12) Flaig, R. W.; Osborn Popp, T. M.; Fracaroli, A. M.; Kapustin, E. A.; Kalmutzki, M. J.; Altamimi, R. M.; Fathieh, F.; Reimer, J. A.; Yaghi, O. M. The Chemistry of CO_2 Capture in an Amine-Functionalized Metal-Organic Framework under Dry and Humid Conditions. *J. Am. Chem. Soc.* **2017**, *139*, 12125−12128.

(13) Carrington, E. J.; McAnally, C. A.; Fletcher, A. J.; Thompson, S. P.; Warren, M.; Brammer, L. Solvent-switchable continuous-breathing behaviour in a diamondoid metal-organic framework and its influence on CO_2 versus CH_4 selectivity. *Nat. Chem.* **2017**, *9*, 882−889.

(14) Gadipelli, S.; Guo, Z. X. Tuning of ZIF-Derived Carbon with High Activity, Nitrogen Functionality, and Yield - A Case for Superior CO_2 Capture. *ChemSusChem* **2015**, *8*, 2123−2132.

(15) Zeng, Y.; Zou, R.; Zhao, Y. Covalent Organic Frameworks for CO_2 Capture. *Adv. Mater.* **2016**, *28*, 2855−2873.

(16) Yao, K. X.; Chen, Y.; Lu, Y.; Zhao, Y.; Ding, Y. Ultra-microporous carbon with extremely narrow pore distribution and very high nitrogen doping for efficient methane mixture gases upgrading. *Carbon* **2017**, *122*, 258−265.

DOI: 10.1021/acs.energyfuels.9b02631
Energy Fuels 2019, 33, 11454−11464

(17) Chang, B.; Shi, W.; Yin, H.; Zhang, S.; Yang, B. Poplar catkin-derived self-templated synthesis of N-doped hierarchical porous carbon microtubes for effective CO_2 capture. *Chem. Eng. J.* **2019**, *358*, 1507−1518.
(18) Hirst, E. A.; Taylor, A.; Mokaya, R. A simple flash carbonization route for conversion of biomass to porous carbons with high CO_2 storage capacity. *J. Mater. Chem. A* **2018**, *6*, 12393−12403.
(19) Wu, Y.; Wang, J.; Muhammad, Y.; Subhan, S.; Zhang, Y.; Ling, Y.; Li, J.; Zhao, Z.; Zhao, Z. Pyrrolic N-enriched carbon fabricated from dopamine-melamine via fast mechanochemical copolymerization for highly selective separation of CO_2 from CO_2/N_2. *Chem. Eng. J.* **2018**, *349*, 92−100.
(20) Park, J.; Jung, M.; Jang, H.; Lee, K.; Attia, N. F.; Oh, H. A facile synthesis tool of nanoporous carbon for promising H_2, CO_2, and CH_4 sorption capacity and selective gas separation. *J. Mater. Chem. A* **2018**, *6*, 23087−23100.
(21) Li, D.; Zhou, J.; Wang, Y.; Tian, Y.; Wei, L.; Zhang, Z.; Qiao, Y.; Li, J. Effects of activation temperature on densities and volumetric CO_2 adsorption performance of alkali-activated carbons. *Fuel* **2019**, *238*, 232−239.
(22) Shao, L.; Sang, Y.; Huang, J. Imidazole-based hyper-cross-linked polymers derived porous carbons for CO_2 capture. *Microporous Mesoporous Mater.* **2019**, *275*, 131−138.
(23) Zhao, H.; Shi, L.; Zhang, Z.; Luo, X.; Zhang, L.; Shen, Q.; Li, S.; Zhang, H.; Sun, N.; Wei, W.; Sun, Y. Potassium Tethered Carbons with Unparalleled Adsorption Capacity and Selectivity for Low-Cost Carbon Dioxide Capture from Flue Gas. *ACS Appl. Mater. Interfaces* **2018**, *10*, 3495−3505.
(24) Chen, C.; Huang, H.; Yu, Y.; Shi, J.; He, C.; Albilali, R.; Pan, H. Template-free synthesis of hierarchical porous carbon with controlled morphology for CO_2 efficient capture. *Chem. Eng. J.* **2018**, *353*, 584−594.
(25) Pei, Y. R.; Choi, G.; Asahina, S.; Yang, J. H.; Vinu, A.; Choy, J. H. A novel geopolymer route to porous carbon: high CO_2 adsorption capacity. *Chem. Commun.* **2019**, *55*, 3266−3269.
(26) Zhou, J.; Li, D.; Wang, Y.; Tian, Y.; Zhang, Z.; Wei, L.; Feng, W. Effect of the Feedstock Type on the Volumetric Low-Pressure CO_2 Capture Performance of Activated Carbons. *Energy Fuels* **2018**, *32*, 12711−12720.
(27) Liu, L.; Xie, Z.-H.; Deng, Q.-F.; Hou, X.-X.; Yuan, Z.-Y. One-pot carbonization enrichment of nitrogen in microporous carbon spheres for efficient CO_2 capture. *J. Mater. Chem. A* **2017**, *5*, 418−425.
(28) Nie, B.; Zhou, C.; Gao, M.; He, D.; Yao, Z.; Liu, Y.; Shen, X.; Wang, X.; Pan, H. Bi-structural fibers of carbon nanotube coated with nitrogen/oxygen dual-doped porous carbon layer as superior sulfur host for lithium-sulfur batteries. *J. Alloys Compd.* **2019**, *797*, 1205−1215.
(29) Wan, L.; Wang, J.; Feng, C.; Sun, Y.; Li, K. Synthesis of polybenzoxazine based nitrogen-rich porous carbons for carbon dioxide capture. *Nanoscale* **2015**, *7*, 6534−6544.
(30) Fayemiwo, K. A.; Vladisavljević, G. T.; Nabavi, S. A.; Benyahia, B.; Hanak, D. P.; Loponov, K. N.; Manović, V. Nitrogen-rich hyper-crosslinked polymers for low-pressure CO_2 capture. *Chem. Eng. J.* **2018**, *334*, 2004−2013.
(31) Cong, H.; Zhang, M.; Chen, Y.; Chen, K.; Hao, Y.; Zhao, Y.; Feng, L. Highly selective CO_2 capture by nitrogen enriched porous carbons. *Carbon* **2015**, *92*, 297−304.
(32) Liu, Y.; Wang, Z.; Teng, W.; Zhu, H.; Wang, J.; Elzatahry, A. A.; Al-Dahyan, D.; Li, W.; Deng, Y.; Zhao, D. A template-catalyzedin situpolymerization and co-assembly strategy for rich nitrogen-doped mesoporous carbon. *J. Mater. Chem. A* **2018**, *6*, 3162−3170.
(33) Kutorglo, E. M.; Hassouna, F.; Beltzung, A.; Kopecký, D.; Sedlářová, I.; Šoóš, M. Nitrogen-rich hierarchically porous polyaniline-based adsorbents for carbon dioxide (CO_2) capture. *Chem. Eng. J.* **2019**, *360*, 1199−1212.
(34) Xing, W.; Liu, C.; Zhou, Z.; Zhang, L.; Zhou, J.; Zhuo, S.; Yan, Z.; Gao, H.; Wang, G.; Qiao, S. Z. Superior CO_2 uptake of N-doped activated carbon through hydrogen-bonding interaction. *Energy Environ. Sci.* **2012**, *5*, 7323−7327.
(35) Liu, M.; Shao, L.; Huang, J.; Liu, Y.-N. O-containing hyper-cross-linked polymers and porous carbons for CO_2 capture. *Microporous Mesoporous Mater.* **2018**, *264*, 104−111.
(36) Zhang, C.; Kong, R.; Wang, X.; Xu, Y.; Wang, F.; Ren, W.; Wang, Y.; Su, F.; Jiang, J.-X. Porous carbons derived from hypercrosslinked porous polymers for gas adsorption and energy storage. *Carbon* **2017**, *114*, 608−618.
(37) Wang, M.; Fan, X.; Zhang, L.; Liu, J.; Wang, B.; Cheng, R.; Li, M.; Tian, J.; Shi, J. Probing the role of O-containing groups in CO_2 adsorption of N-doped porous activated carbon. *Nanoscale* **2017**, *9*, 17593−17600.
(38) Das, S. K.; Bhanja, P.; Kundu, S. K.; Mondal, S.; Bhaumik, A. Role of Surface Phenolic-OH Groups in N-Rich Porous Organic Polymers for Enhancing the CO_2 Uptake and CO_2/N_2 Selectivity: Experimental and Computational Studies. *ACS Appl. Mater. Interfaces* **2018**, *10*, 23813−23824.
(39) Liao, P.-Q.; Chen, H.; Zhou, D.-D.; Liu, S.-Y.; He, C.-T.; Rui, Z.; Ji, H.; Zhang, J.-P.; Chen, X.-M. Monodentate hydroxide as a super strong yet reversible active site for CO_2 capture from high-humidity flue gas. *Energy Environ. Sci.* **2015**, *8*, 1011−1016.
(40) Li, H.; Meng, B.; Mahurin, S. M.; Chai, S.-H.; Nelson, K. M.; Baker, D. C.; Liu, H.; Dai, S. Carbohydrate based hyper-crosslinked organic polymers with −OH functional groups for CO_2 separation. *J. Mater. Chem. A* **2015**, *3*, 20913−20918.
(41) Bien, C. E.; Chen, K. K.; Chien, S.-C.; Reiner, B. R.; Lin, L.-C.; Wade, C. R.; Ho, W. S. W. Bioinspired Metal-Organic Framework for Trace CO_2 Capture. *J. Am. Chem. Soc.* **2018**, *140*, 12662−12666.
(42) (a) Zhang, K.; Han, L.; Froimowicz, P.; Ishida, H. A Smart Latent Catalyst Containing o-Trifluoroacetamide Functional Benzoxazine: Precursor for Low Temperature Formation of Very High Performance Polybenzoxazole with Low Dielectric Constant and High Thermal Stability. *Macromolecules* **2017**, *50*, 6552−6560. (b) Liu, X.; Li, Z.; Zhan, G.; Wu, Y.; Zhuang, Q. Bio-based benzoxazines based on sesamol: Synthesis and properties. *J. Appl. Polym. Sci.* **2019**, *136*, 48255.
(43) Liu, X.; Zhang, R.; Li, T.; Zhu, P.; Zhuang, Q. Novel Fully Biobased Benzoxazines from Rosin: Synthesis and Properties. *ACS Sustainable Chem. Eng.* **2017**, *5*, 10682−10692.
(44) Zhang, Y.; Liu, X.; Zhan, G.; Zhuang, Q.; Zhang, R.; Qian, J. Study on the synergistic anticorrosion property of a fully bio-based polybenzoxazine copolymer resin. *Eur. Polym. J.* **2019**, *119*, 477−486.
(45) Zhang, K.; Cai, R.; Zhuang, Q.; Liu, X.; Yang, G.; Han, Z. High performance crosslinked system based on reaction of benzoxazine with benzoxazole. *J. Polym. Sci., Part A: Polym. Chem.* **2014**, *52*, 1514−1518.
(46) Zhang, K.; Zhuang, Q.; Liu, X.; Yang, G.; Cai, R.; Han, Z. A New Benzoxazine Containing Benzoxazole-Functionalized Polyhedral Oligomeric Silsesquioxane and the Corresponding Polybenzoxazine Nanocomposites. *Macromolecules* **2013**, *46*, 2696−2704.
(47) Zhang, K.; Zhuang, Q.; Liu, X.; Cai, R.; Yang, G.; Han, Z. Synthesis and copolymerization of benzoxazines with low-dielectric constants and high thermal stability. *RSC Adv.* **2013**, *3*, 5261−5270.
(48) Zhang, K.; Zhuang, Q.; Zhou, Y.; Liu, X.; Yang, G.; Han, Z. Preparation and properties of novel low dielectric constant benzoxazole-based polybenzoxazine. *J. Polym. Sci., Part A: Polym. Chem.* **2012**, *50*, 5115−5123.
(49) Kresse, G.; Hafner, J. Ab initiomolecular dynamics for liquid metals. *Phys. Rev. B* **1993**, *47*, 558−561.
(50) Kresse, G.; Furthmüller, J. Efficient iterative schemes for ab initio total-energy calculations using a plane-wave basis set. *Phys. Rev. B* **1996**, *54*, 11169−11186.
(51) Blöchl, P. E. Projector augmented-wave method. *Phys. Rev. B* **1994**, *50*, 17953−17979.
(52) Perdew, J. P.; Burke, K.; Ernzerhof, M. Generalized gradient approximation made simple. *Phys. Rev. Lett.* **1996**, *77*, 3865−3868.

DOI: 10.1021/acs.energyfuels.9b02631
Energy Fuels 2019, 33, 11454−11464

(53) Grimme, S. Semiempirical GGA-type density functional constructed with a long-range dispersion correction. *J. Comput. Chem.* **2006**, *27*, 1787−99.
(54) Kou, J.; Sun, L.-B. Fabrication of nitrogen-doped porous carbons for highly efficient CO_2 capture: rational choice of a polymer precursor. *J. Mater. Chem. A* **2016**, *4*, 17299−17307.
(55) Ashourirad, B.; Sekizkardes, A. K.; Altarawneh, S.; El-Kaderi, H. M. Exceptional Gas Adsorption Properties by Nitrogen-Doped Porous Carbons Derived from Benzimidazole-Linked Polymers. *Chem. Mater.* **2015**, *27*, 1349−1358.
(56) To, J. W. F.; He, J.; Mei, J.; Haghpanah, R.; Chen, Z.; Kurosawa, T.; Chen, S.; Bae, W.-G.; Pan, L.; Tok, J. B.-H.; Wilcox, J.; Bao, Z. Hierarchical N-Doped Carbon as CO_2 Adsorbent with High CO_2 Selectivity from Rationally Designed Polypyrrole Precursor. *J. Am. Chem. Soc.* **2016**, *138*, 1001−1009.
(57) Sevilla, M.; Valle-Vigón, P.; Fuertes, A. B. N-Doped Polypyrrole-Based Porous Carbons for CO2Capture. *Adv. Funct. Mater.* **2011**, *21*, 2781−2787.
(58) Wan, L.; Wang, J.; Sun, Y.; Feng, C.; Li, K. Polybenzoxazine-based nitrogen-containing porous carbons for high-performance supercapacitor electrodes and carbon dioxide capture. *RSC Adv.* **2015**, *5*, 5331−5342.
(59) Wu, J. Y.; Mohamed, M. G.; Kuo, S. W. Directly synthesized nitrogen-doped microporous carbons from polybenzoxazine resins for carbon dioxide capture. *Polym. Chem.* **2017**, *8*, 5481−5489.
(60) Wang, S.; Li, W.-C.; Zhang, L.; Jin, Z.-Y.; Lu, A.-H. Polybenzoxazine-based monodisperse carbon spheres with low-thermal shrinkage and their CO_2 adsorption properties. *J. Mater. Chem. A* **2014**, *2*, 4406−4412.
(61) Nandi, M.; Okada, K.; Dutta, A.; Bhaumik, A.; Maruyama, J.; Derks, D.; Uyama, H. Unprecedented CO_2 uptake over highly porous N-doped activated carbon monoliths prepared by physical activation. *Chem. Commun.* **2012**, *48*, 10283−10285.
(62) Bae, Y. S.; Snurr, R. Q. Development and evaluation of porous materials for carbon dioxide separation and capture. *Angew. Chem., Int. Ed.* **2011**, *50*, 11586−96.
(63) Bai, R.; Yang, M.; Hu, G.; Xu, L.; Hu, X.; Li, Z.; Wang, S.; Dai, W.; Fan, M. A new nanoporous nitrogen-doped highly-efficient carbonaceous CO_2 sorbent synthesized with inexpensive urea and petroleum coke. *Carbon* **2015**, *81*, 465−473.
(64) Yuan, B.; Wu, X.; Chen, Y.; Huang, J.; Luo, H.; Deng, S. Adsorption of CO_2, CH_4, and N_2 on Ordered Mesoporous Carbon: Approach for Greenhouse Gases Capture and Biogas Upgrading. *Environ. Sci. Technol.* **2013**, *47*, 5474−5480.
(65) Wei, J.; Zhou, D.; Sun, Z.; Deng, Y.; Xia, Y.; Zhao, D. A Controllable Synthesis of Rich Nitrogen-Doped Ordered Mesoporous Carbon for CO_2 Capture and Supercapacitors. *Adv. Funct. Mater.* **2013**, *23*, 2322−2328.
(66) Ma, X.; Cao, M.; Hu, C. Bifunctional HNO_3 catalytic synthesis of N-doped porous carbons for CO_2 capture. *J. Mater. Chem. A* **2013**, *1*, 913−918.
(67) Sevilla, M.; Fuertes, A. B. Sustainable porous carbons with a superior performance for CO_2 capture. *Energy Environ. Sci.* **2011**, *4*, 1765−1771.
(68) Wahby, A.; Ramos-Fernández, J. M.; Martínez-Escandell, M.; Sepúlveda-Escribano, A.; Silvestre-Albero, J.; Rodríguez-Reinoso, F. High-surface-area carbon molecular sieves for selective CO_2 adsorption. *ChemSusChem* **2010**, *3*, 974−981.
(69) Kemp, K. C.; Chandra, V.; Saleh, M.; Kim, K. S. Reversible CO_2 adsorption by an activated nitrogen doped graphene/polyaniline material. *Nanotechnology* **2013**, *24*, 235703−235711.

DOI: 10.1021/acs.energyfuels.9b02631
Energy Fuels 2019, 33, 11454−11464